POTSDAM-INSTITUT FÜR
KLIMAFOLGENFORSCHUNG

Using Causal Effect Networks to analyze different Arctic drivers of mid-latitude winter circulation

Marlene Kretschmer[*1,2], Dim Coumou[1], Jonathan F. Donges[1,3], Jakob Runge[1,4]

[1]Potsdam Institute for Climate Impact Research, Germany

[2]Department of Mathematics, University of Potsdam, Germany

[3]Stockholm Resilience Centre, Sweden

[4]Department of Physics, Humboldt University Berlin, Germany

*Corresponding author: M. Kretschmer, kretschmer@pik-potsdam.de, Telegrafenberg A62, 14473 Potsdam, Germany

Abstract

In the past years, the northern hemisphere mid-latitudes have suffered from severe winters like the extreme 2012/2013 winter in Eastern USA. These cold spells were linked to a meandering upper tropospheric jet stream pattern and a negative Arctic Oscillation Index (AO). However, the nature of the drivers behind these circulation patterns remains controversial. Various studies have proposed different mechanisms related to changes in the Arctic, most of them related to a reduction in sea ice concentrations or increasing Eurasian snow cover. Here, a novel type of time series analysis, called *Causal Effect Networks* (CEN) based on graphical models is introduced to assess causal relationships and their time-delays between different processes. The effect of different Arctic actors on winter circulation on weekly to

monthly time-scales is studied and robust network patterns are found. Barents and Kara sea ice concentrations are detected to be important external drivers of the mid-latitude circulation, influencing winter AO via tropospheric mechanisms and through processes involving the Stratosphere. Eurasia snow cover is also detected to have a causal effect on sea level pressure in Asia, but its exact role on AO remains unclear. The CEN approach presented in this study overcomes some difficulties in interpreting correlation analyses, complements model experiments for testing hypotheses involving teleconnections, and can be used to assess their validity. Our findings confirm that sea ice concentrations in autumn in the Barents and Kara Seas are an important driver of winter circulation in the mid-latitudes.

1. Introduction

The recent cold winters in North America and Eurasia were characterized by a meandering jet stream pattern which allowed cold arctic air to reach lower latitudes [*Cohen et al.*, 2014b]. Moreover, these winters were dominated by a negative phase of the Arctic Oscillation Index (AO), which is usually associated with pronounced meridional wind patterns, whereas in a positive AO phase strong zonal flow dominates the wind field. Although a negative AO and meandering flow patterns have been linked to surface extremes [*Thompson*, 2001; *Coumou et al.*, 2014; *Screen and Simmonds*, 2014], it is intensively discussed what the mechanisms behind AO variability are.

Classical atmosphere dynamic theories relate a meandering jet stream structure to above normal sea surface temperatures in the tropical Pacific [*Palmer and Mansfeld*, 1984; *Palmer and*

Owen, 1986; *Trenberth et al.*, 1998]. Warming of the tropical Pacific intensifies evaporation, increasing thunderstorm activity in that region. The associated latent heat release can then trigger large-amplitude planetary waves affecting the mid-latitude flow.

In contrast, some recently proposed theories focus on the polar region, claiming that anomalous atmospheric circulations can be linked to low Arctic sea ice concentrations as observed during the last two decades [*Petoukhov and Semenov*, 2010; *Francis and Vavrus*, 2012; *Jaiser et al.*, 2012; *Handorf et al.*, 2015]. A reduction in sea ice cover in summer leads to the ocean taking up more energy in this season. Since sea ice works as an insulating shield blocking the ocean-atmosphere interaction, less sea ice in autumn and early winter facilitates larger heat fluxes from the relatively warm ocean into the atmosphere. Kim et al. focus on the Barents and Kara Seas in particular and argue that reduction in sea ice concentration preferentially in this area lead to a weakened AO via the stratospheric polar vortex [*Kim et al.*, 2014]. They link the additional heat release to the atmosphere caused by sea ice loss in early winter to anomalously high geopotential heights over the Barents and Kara Sea region in addition to lower than normal geopotential heights over Northern Western Europe and Eastern Asia. This observed wave-like structure indicates upward propagation of large scale planetary waves into the Stratosphere, interfering with the predominantly zonal flow in the lower Stratosphere. As a result, the stratospheric zonal flow weakens and the geopotential heights and wind anomalies descend to the Troposphere, which is also called a “breakdown” of the polar vortex. As a consequence, cold Arctic air reaches lower latitudes thereby forming large meanders. Those pressure anomalies, respectively meandering of the jet stream, are then most often reflected in a negative phase of AO. Kim et al. (2104) base their analysis on theoretical physical considerations and observational

64 data. They validate their results using climate model simulations, which reproduce similar
65 patterns, supporting their proposed theory.

66 A similar mechanism was proposed by Cohen et al. who linked increased fall snow cover in
67 Eurasia to changes in surface pressure anomalies, causing a likewise chain of effects [*Cohen et*
68 *al.*, 2007, 2013, 2014a]. Based on observational data and correlation analysis they hypothesize
69 that an extended Eurasian snow cover in fall, likely resulting from decreasing Arctic sea ice,
70 leads to increasing sea level pressures over Central Asia in early winter. As a result a disturbed
71 pressure pattern in the polar region is observed, leading to increased vertical wave activity and
72 poleward heat flux. This is followed by anomalously high geopotential heights in the
73 Stratosphere, associated with stratospheric warming and weakening of the polar vortex, and
74 respectively a negative surface AO as described by Baldwin and Dunkerton (1999).

75 In order to study the atmospheric response to changes in the Arctic, different methods have
76 been used. Cross-correlation analysis is widely applied to detect linear relationships and their
77 time delays between different processes [*Polvani and Waugh*, 2004; *Cohen et al.*, 2014a].
78 However, correlation can be highly biased by auto-correlation effects, by indirect connections
79 via a third process, or by a common driver leading to non-causal, spurious correlations that
80 limits its interpretability [*Runge et al.*, 2014]. Also, it does not give any answer on the direction
81 of the relationship, such that it is not an adequate tool to study causal effects. Therefore climate
82 models are used, to investigate atmospheric changes due to a controlled perturbation of the
83 system [*Deser et al.*, 2010; *Petoukhov and Semenov*, 2010; *Handorf et al.*, 2015]. This approach
84 allows interpreting results as causal effects forced by the input data. However, conclusions are
85 strictly limited to the extent of the physical realism of the climate model used. It remains

questionable whether models capture important processes like ocean-ice feedbacks [*Tremblay et al.*, 2007], land-snow interactions [*Furtado et al.*, 2015], troposphere-stratosphere interactions [*Manzini et al.*, 2014] and Rossby wave propagation [*Gray et al.*, 2014] accurately. Thus, both climate model experiments and correlation analysis of observational data are restricted in their interpretability [*Barnes and Screen*, 2015].

Here we analyze observational data with a novel method based on graphical models called *Causal Effect Networks (CEN)*. This method overcomes spurious correlations due to autocorrelation, indirect effects or common drivers (at least among the observed variables included) using a causal discovery algorithm as proposed by Runge et al. (2012a, 2012b, 2014). This algorithm is a modified version of the PC-algorithm [*Spirtes et al.*, 2000] (named after its inventors Peter Spirtes and Clark Glymour) which has first been applied to climate research by Ebert-Uphoff and Deng [*Ebert-Uphoff and Deng*, 2012] to study interactions between major climate modes. Causal discovery approaches have since then been used to study atmospheric flows [*Deng and Ebert-Uphoff*, 2014], causal relationships in the Walker Cell in the Tropics [*Runge et al.*, 2014], the monsoonal dynamics in the Pacific-Indian Ocean [*Runge et al.*, 2015] and decadal ocean circulation in the Atlantic [*Schleussner et al.*, 2014].

The aim of this paper is to explain how to apply this method and show how it can be used for hypothesis testing in the context of teleconnections in climate research. We apply CEN to observational and reanalysis data in order to understand how different mechanisms which might cause a negative AO in winter are causally related with each other. In this study, we limit ourselves to testing a set of proposed Arctic mechanisms. In contrast to tropical mechanisms, those operate on similar sub-seasonal timescales, which facilitates a simultaneous analysis.

The article is structured as follows: In section 2 the data selection is motivated and section 3 gives a detailed description of the two different steps of the CEN-algorithm on the basis of an example. In section 4 the sensitivity of the parameter settings and temporal resolution is analyzed and structure and robustness of the graphs are discussed in the framework of the tested hypothesis. Finally, in section 5 we conclude and assess the potentials and limitations of the presented method.

2. Data

Different actors can influence mid-latitudinal winter circulation. The first step of our analysis is hence to come up with a reasonable choice of processes which are expected to be relevant for the analysis. This includes the decision for physical variables which should serve as proxies for the considered processes, the selection of suitable data sources and a reasonable time resolution of the data.

As stated, we limit the analysis to Arctic processes and follow Kim et al. (2014) and Cohen et al. (2014) with respect to data selection. We therefore include Barents and Kara sea ice concentrations (BK-SIC) as well as Eurasia snow cover (EA-snow) in our analysis, as possible causal drivers of a negative Arctic Oscillation Index (AO). We further include sea level pressure in the Ural Mountains region (Ural-SLP) as defined in [*Cohen et al.*, 2014] and sea level pressure in the Lake Baikal area as a proxy for Siberian High variability (Sib-SLP). Following Kim et al. and Cohen et al. we include the zonally averaged poleward heat flux v*T* at 100 mb (v-flux) to

129 capture the Troposphere-Stratosphere coupling. This is a widely used proxy for vertical wave
130 activity, whereby v denotes the meridional wind velocity, T stands for temperature and the
131 asterisk denotes deviations from the zonal mean [*Polvani and Waugh*, 2004; *Dunn-Sigouin and*
132 *Shaw*, 2015]. There are many possible ways to describe polar vortex activity (PoV), but for
133 consistency with Kim et al. (2014) and Cohen et al. (2014) we calculate geopotential height
134 anomalies poleward of 65°N, averaged over pressure levels from 10mb to 100mb to define the
135 strength of the stratospheric polar vortex. Eurasia snow data is described in [*Robinson et al.*,
136 1993] and is provided by NOAA[1]. Sea ice concentration data was taken from the Nimbus-7
137 SMMR and DMSP SSM/I-SSMIS passive microwave data set provided by the National Snow & Ice
138 Data Center[2]. The Arctic Oscillation Index (AO) is provided by NOAA[3] and for the remaining
139 variables we used ERA-Interim reanalysis data[4].

140 In summary, our analysis contains seven different actors (Tab. 1): Barents and Kara sea ice
141 concentrations (BK-SIC), Eurasia snow cover (EA-snow), the Arctic Oscillation Index (AO), vertical
142 wave activity (v-flux), polar vortex strength (PoV), sea level pressure over the Ural Mountains
143 (Ural-SLP) and Siberian High activity (Sib-SLP). For each variable we consider the time-period
144 01/1979-12/2014, which is most reliable in the reanalysis due to availability of satellite data.

145 We calculate monthly means of daily data for each variable as we are testing mechanisms which
146 are expected to act on monthly time scales. Thereby we perform linear interpolation of the

[1] http://gis.ncdc.noaa.gov/all-records/catalog/search/resource/details.page?id=gov.noaa.ncdc:C00756

[2] http://nsidc.org/data/nsidc-0051

[3] http://www.cpc.ncep.noaa.gov/products/precip/CWlink/daily_ao_index/ao.shtml

[4] http://apps.ecmwf.int/datasets/data/interim-full-daily/

147 snow data and for some years of the sea ice concentration data set, where daily data is not
148 available. To gain additional information on the time-scale of the considered processes we
149 perform additional analysis using half-month means as well as quarter-month means of every
150 variable (Fig. 1). For half-monthly data we take the mean from the 1^{st} - 15^{th} and from the 16^{th}-
151 30^{th} of each month and for February from 1^{st} - 14^{th} and 15^{th} - 28^{th} respectively (thus ignoring the
152 31^{th} of all applicable months as well as the 29^{th} of February in leap years). To construct quarter-
153 monthly time series we calculate the mean from 1^{st} - 7^{th}, 9^{th} - 15^{th}, 16^{th} - 22^{th} and 24^{th} - 30^{th}
154 (neglecting hence the 8^{th}, 23^{th} and 31^{th} of all applicable months) and for February from 1^{st} - 7^{th},
155 8^{th} - 14^{th}, 15^{th} - 21^{th} and 22^{th} - 28^{th} respectively. This approach has the advantage that the
156 different time-series are still in sync with each other facilitating the comparison of associated
157 CENs.

158 For each variable and time-resolution we calculate climatological anomalies (observed value
159 minus the multi-year mean), from which we then compute the area-weighted spatial average
160 over the defined region (see last column in Tab. 1). This way we create single time-series for
161 each time-resolution and each actor (see Fig. 2 for monthly data). Since CEN construction
162 requires stationary time-series, we remove the linear trend if present. For our analysis this is
163 only the case for Barents and Kara sea ice concentrations (BK-SIC). Additionally we change the
164 sign of PoV, such that positive values (negative geopotential height anomalies) indicate a strong
165 polar vortex.

166

167

3. Method

The Causal Effect Networks approach is based on two steps: (1) Reconstructing the causal parents of each actor using a causal discovery algorithm [*Runge et al.*, 2012a, 2012b, 2014], which is a modification of the PC-algorithm [*Spirtes et al.*, 2000] for time series. As explained in the following, this step is based on iterative conditional independence tests using partial correlation. (2) In a second step, the strength of causal links is quantified using a linear version of Pearl's causal effect measures [*Pearl*, 2013]. Thereby the parents are used in a multiple linear regression analysis to test the significance and strength of causal dependencies between all pairs of actors at a range of time-lags.

Here we use a linear approach to estimate and interpret causal links, but the two-step procedure of causal reconstruction and quantification can also be embedded in an information-theoretic framework to study causal information transfer accounting for nonlinear relationships between variables. For a detailed explanation of the method, including a mathematical analysis as well as numerical testing, we refer to Runge et al. (2012a, 2012b, 2014). All calculations presented in this study were performed using the Python package TiGraMITe *(Time series graph based Measures of Information Transfer)* which provides the CEN-algorithm and is freely available[5].

In the following we explain how to apply CEN to test causality of the hypotheses discussed in the introduction.

[5] https://www.pik-potsdam.de/members/jakrunge

Step 1: Detecting Causal Effects

The first step of the CEN-algorithm aims to find causal relationships between the different actors and their associated time lags. The scope of this step is to identify past processes which directly influence each actor. We call those processes the parents of an actor and they will be used later to determine the actual strength and the sign of the causal relationships.

Cross-correlation can give a first impression of the pairwise linear relationship between two processes X and Y. However, it is not able to identify causal links because the bivariate analysis can be biased by autocorrelation of the two variables, by common drivers or by indirect links via a third process Z (Fig. 3a, b, c). For example cross-correlation of two independent processes X and Y can be high if one of the processes is strongly auto-correlated (Fig. 3a). Also, imagine that Z causes X and Y (Fig. 3c) then cross-correlation analysis would find a strong correlation between X and Y even though there in no direct link between them. In order to detect causal links, a multivariate analysis is required which takes all potential actors into account.

Recall that two processes X and Y are conditionally independent given a third process Z if $P(X \cap Y|Z)=P(X|Z)P(Y|Z)$, whereby P denotes the probability function. In the linear case this can be tested by removing the linear influence of Z from both X and Y and testing for the correlation between their residuals (partial correlation). In the previous case (Fig. 3c), X and Y would then be conditionally independent given Z. In the example illustrated in Fig. 3b, process X causes Z which in turn influences Y. Process X and Y are thus conditionally independent given Z and a high correlation coefficient between X and Y only occurs due to the indirect link via Z.

This section discusses how the CEN-algorithm uses iterative partial correlations to identify non-causal correlations as depicted in Fig. 3. The extent to which such a data-based analysis allows to conclude on a physical causal mechanism depends on the included variables, time resolution of the data and assumptions such as stationarity. Two free parameters are involved: the significance level α for the partial correlation tests and the maximum time delay $\tau_{max.}$

Calculating the parent processes

As an illustrative example, we start with finding those processes on a monthly time-scale among our actors which have a direct causal effect on the winter (December, January, February) polar vortex (PoV). We look at the monthly time-series for every actor (Fig. 2) having thus a sample-length of 108 time-steps. We define a two-sided significance level α=0.01 and a maximum time-lag of τ_{max}=3 months implying that parent processes more than three months ago or those with a significance below 99% will be neglected.

First, for every actor X the cross-correlation function $\rho(X_{t-\tau}, PoV_t)$ is calculated for time shifts of τ=1 up to the maximum time-shift τ_{max}=3 months. Note that, if we study causal effects *on* winter PoV, this implies that the monthly time-series PoV_t only consists of winter data but the lagged or driving variable contains data from other seasons (in particular autumn but also summer when τ>3). Here the expression "driver" is used in its statistical meaning of being conditional-dependent and shifted in time. For τ=1 the expression $\rho(X_{t-1},PoV_t)$ denotes the Pearson correlation coefficient of November-December-January data of process X and December-January-February data of PoV (see Fig. 4) whereas for τ=3 the linear influence of the three months shifted September-October-November data of actor X on PoV in winter (DJF) is

measured. For example, for the influence of Eurasia snow cover (X=EA-snow) on the polar vortex with a time delay of $\tau=1$ we obtain:

$$\rho(\text{EA-snow}_{t-1}, \text{PoV}_t) = -0.262$$

which is significant at the $\alpha=0.01$ level. This indicates that there is a negative linear relationship between early winter (NDJ) snow and the winter polar vortex. This seems reasonable since a large snow cover in Eurasia is indicated to induce a weakened polar vortex [*Cohen et al.*, 2014]. The cross-correlation function is now calculated and evaluated for every actor $X \in \{\text{BK-SIC}_{t-\tau}, \text{EA-snow}_{t-\tau}, \text{AO}_{t-\tau}, \text{v-flux}_{t-\tau}, \text{PoV}_{t-\tau}, \text{Sib-SLP}_{t-\tau}, \text{Ural-SLP}_{t-\tau}\}$ and every time-lag $\tau \in \{1,2,3\}$. We find that besides EA-snow (with $\tau=1$), also Ural-SLP (with $\tau=1$ and $\tau=2$), AO (with $\tau=1$), PoV (with $\tau=1$) and v-flux (with $\tau=1$) are significantly correlated with winter PoV. Sorted by the strength of correlation starting with the strongest in absolute value, the set of potential parent-processes of PoV in this zeroth iteration step without any conditioning is:

$$\mathbf{P^0} = \{\text{v-flux}_{t-1}, \text{PoV}_{t-1}, \text{Ural-SLP}_{t-1}, \text{Ural-SLP}_{t-2}, \text{AO}_{t-1}, \text{EA-snow}_{t-1}\}.$$

To test these potential drivers for conditional independence, we next calculate partial correlations:

$$\rho(X_{t-\tau}, Y_t | \mathbf{Z})$$

which measure the linear influence from process X on Y, excluding the influence of some set of variables **Z.** This thus checks if X and Y are conditionally independent given **Z**. We choose **Z** as a subset of $\mathbf{P^0}$ such that **Z** denotes a set of other processes which potentially influences the bivariate correlation coefficient $\rho(X_{t-\tau}, Y_t)$. In each iteration step $\mathbf{P^1}$, $\mathbf{P^2}$, ... we condition on a new

Z, whereby the algorithm first takes only one condition and starts with the process which is strongest correlated (in absolute value) with process Y. Then the dimension of the subset selected from the remaining parents is increased and different two-dimensional conditions are tested and so on for higher dimensions. If the partial correlation significance test of a pair $X_{t-\tau}$ and Y_t is non-significant given **Z**, the process $X_{t-\tau}$ is removed from the set of potential parents. If, however, the partial correlation $\rho(X_{t-\tau},Y_t|\mathbf{Z})$ remains significant for all tested **Z**, then actor X is considered to directly influence Y with a time-lag of τ.

Returning to our example, we first test condition $\mathbf{Z}=\{\text{v-flux}_{t-1}\}$ and find:

$$\rho(\text{EA-snow}_{t-1}, \text{PoV}_t \mid \text{v-flux}_{t-1}) = -0.147$$

which is not significantly different from zero at our chosen level and hence we find that EA-snow and PoV are conditionally independent (at a time-delay of one month) if the influence of v-flux from the same time shift is excluded. We thus conclude that there is no direct influence from EA-snow on PoV with a delay of one month and that the significant correlation between them $\rho(\text{EA-snow}_{t-1}, \text{PoV}_t) = -0.261$ is due to the influence of v-flux. For example, EA-snow could be linked to PoV indirectly via v-flux (as in Fig. 3b). On the other hand, if we take $X=\text{Ural-SLP}_{t-1} \in \mathbf{P^0}$ and condition on the same $\mathbf{Z}=\{\text{v-flux}_{t-1}\}$ we find

$$\rho(\text{Ural-SLP}_{t-1}, \text{PoV}_t \mid \text{v-flux}_{t-1}) = -0.281$$

which is still significantly different from zero. In other words, the linear influence of Ural-SLP_{t-1} on PoV_t cannot exclusively be explained by the linear influence of v-flux.

We calculate partial correlations for all the elements from $\mathbf{P^0}$ conditioning on $\mathbf{Z}$={v-flux$_{t-1}$} and find that some of them are conditionally independent from PoV given v-flux$_{t-1,}$ which can thus be neglected as potential drivers of winter PoV. This way we obtain a much smaller set of potential parent processes of PoV:

$$\mathbf{P^1} = \{\text{v-flux}_{t-1}, \text{PoV}_{t-1}, \text{Ural-SLP}_{t-1}\} \subset \mathbf{P^0}.$$

Now the algorithm proceeds by conditioning on the process which was second strongest correlated with PoV, i.e. $\mathbf{Z}$={PoV$_{t-1}$}. We thus check if some of the potential drivers of PoV only occur due to the auto-correlation of PoV. Calculating partial correlations of the elements of $\mathbf{P^1}$ conditioning on $\mathbf{Z}$={PoV$_{t-1}$} gives only values significantly different from zero such that $\mathbf{P^2} = \mathbf{P^1}$. The last possibility of picking only one condition is $\mathbf{Z}$={Ural-SLP$_{t-1}$}, where we find again that all the partial correlations remain significantly different from zero such that $\mathbf{P^3} = \mathbf{P^2} = \mathbf{P^1}$ Sorting the elements by the strength of their partial correlation value in the last iteration step we have:

$$\mathbf{P^3} = \{\text{v-flux}_{t-1}, \text{Ural-SLP}_{t-1}, \text{PoV}_{t-1}\}.$$

Now we increase the dimension of $\mathbf{Z}$ and condition on two possible drivers from $\mathbf{P^3}$. Thus we start with $\mathbf{Z}$ ={v-flux$_{t-1}$, Ural-SLP$_{t-1}$} $\subset \mathbf{P^3}$ and calculate:

$$\rho(\text{PoV}_{t-1}, \text{PoV}_t \mid \text{v-flux}_{t-1}, \text{Ural-SLP}_{t-1}) = 0.268$$

which is still significantly different from zero. When testing for the other possibilities ($\mathbf{Z}$={v-flux$_{t-1}$, PoV$_{t-1}$} and $\mathbf{Z}$={Ural-SLP$_{t-1,}$ PoV$_{t-1}$}), the partial correlations remain significant. Since there are no more combinations for choosing $\mathbf{Z}$ the algorithm converges and stops.

We have now found the set of direct drivers of winter PoV (relative to the variables taken into account), which we call its parents denoted by:

$$\boldsymbol{\mathcal{P}}_{\text{PoV}} = \{\text{v-flux}_{t-1}, \text{Ural-SLP}_{t-1}, \text{PoV}_{t-1}\}.$$

In other words we found that (given the settings of $\tau_{max}=3$ and $\alpha=0.01$) winter polar vortex (PoV) is directly driven by itself with a delay of one month and by vertical wave activity (v-flux) and pressure variability in the Ural Mountains region (Ural-SLP) with a delay of one month, but is (linearly) conditionally independent of all other processes.

The procedure described for PoV is performed for all actors yielding a set of parents for every actor (see Tab. 2):

$$\boldsymbol{\mathcal{P}} = \{\boldsymbol{\mathcal{P}}_{\text{AO}}, \boldsymbol{\mathcal{P}}_{\text{BK-SIC}}, \boldsymbol{\mathcal{P}}_{\text{EA-snow}}, \boldsymbol{\mathcal{P}}_{\text{v-flux}}, \boldsymbol{\mathcal{P}}_{\text{PoV}}, \boldsymbol{\mathcal{P}}_{\text{Sib-SLP}}, \boldsymbol{\mathcal{P}}_{\text{Ural-SLP}}\}.$$

Note that the interpretation of the significance level α as the probability of false rejections of the hypothesis of a non-causal link is not strictly valid here since we tested every possible link multiple times by conditioning on different processes (see discussion section).

Step 2: Quantifying Causal Effects

In the second step, we use the sets of parents to determine the strength of causal relationships. The case of $\tau=0$, i.e., when there is no time shift between the actors was omitted when calculating the parents. In this step we will nevertheless quantify the significant instantaneous relationships conditional on the parents. As stated above, such contemporaneous links can in

general not be interpreted in a causal way. Some might turn out to be causal parents at a higher time resolution, but some might be just due to excluded common drivers. We address this issue later by studying different time lags.

As mentioned, the set of derived parents depends on the significance level α, which here is, however, not well interpretable due to the multiple testing problem. In order to better assess significance, we therefore test every possible combination of actors and time-lags again (including links from parents) using the causal parents as a conditioning set.

In general, multiple linear regression can be used to measure the influence a system of variables (the independent variables) has on a different (dependent) variable. However, it can often be challenging to define a set of independent variables which can explain the dependent variable. The list of causal parents provides a reasonable choice for those variables with their associated time-lags. We calculate the link strength using standardized multiple linear regression coefficients based on our list of parents for the case of α=0.01 and up to a maximum lag of τ_{max}=3. We found that PoV is influenced from the past by $\mathcal{P}_{\text{PoV}} = \{\text{v-flux}_{t-1}, \text{Ural-SLP}_{t-1}, \text{PoV}_{t-1}\}$. To calculate if process X significantly influences PoV with a time-lag of $\tau \geq 0$ we formulate the standardized linear regression model

$$\text{PoV}^*_t = \beta_0 + \beta_1 \text{v-flux}^*_{t-1} + \beta_2 \text{Ural-SLP}^*_{t-1} + \beta_3 \text{PoV}^*_{t-1} + \beta_4 X^*_{t-\tau} + \varepsilon.$$

Here the beta coefficients β_i with $i \in \{0,1,2,3,4\}$ denote the standardized regression coefficients, ε stands for the error term and the asterisk indicates that the time-series have been normalized and standardized. The regression coefficients express how much the different independent variables contribute to variability in PoV in terms of standard deviations. Interpreted causally

[*Pearl*, 2013], this means that if X is increased by one standard-deviation keeping the other variables fixed, then PoV increases by β_4 standard-deviations. The β-coefficient of X is tested for significance at $\alpha=0.01$ with the null-hypothesis $\beta=0$, which would mean that variable X does not contribute significantly to the dependent variable PoV.

To test if, for example, X=EA-snow significantly influences winter PoV with a delay of one month $\tau=1$ we calculate the standardized linear regression model and choose EA-snow $_{t-1}$ as well as the parents of PoV as independent variables to explain PoV:

$$\text{PoV}^*_t = \beta_0 + \beta_1 \text{v-flux}^*_{t-1} + \beta_2 \text{Ural-SLP}^*_{t-1} + \beta_3 \text{PoV}^*_{t-1} + \beta_4 \text{EA-snow}^*_{t-\tau} + \varepsilon$$

We get $\beta_4 = -0.076$ which is not significant at the $\alpha=0.01$ level such that the influence from EA-snow on PoV with a delay of one month is considered to be absent. If we, however, calculate the influence of v-flux with $\tau=1$ (which is also in $\boldsymbol{\mathcal{P}}_{\text{Pov}}$) on winter PoV we obtain a significant beta coefficient $\beta_1 = -0.514$. Thus, v-flux is concluded to be causally influencing the winter polar vortex with a delay of one month and with a strength of $\beta_1 = -0.514$, i.e., a one-standard deviation increase in v-flux leads to a negative change of about half a standard deviation in PoV.

We test the influence of every actor $X \in \{\text{BK-SIC}_{t-\tau}, \text{EA-snow}_{t-\tau}, \text{AO}_{t-\tau}, \text{v-flux}_{t-\tau}, \text{PoV}_{t-\tau}, \text{Sib-SLP}_{t-\tau}, \text{Ural-SLP}_{t-\tau}\}$ and every time-lag $\tau \in \{0,1,2,3\}$ on PoV as well as on every other actor in form of standardized linear regression. The remaining significant links form our *Causal Effect Network*.

Note, that it is possible that in this step significant direct links are identified which had been rejected in the first step. Nevertheless, by testing every potential link again, we can better interpret the statistical meaning of α as the probability of falsely rejecting the null hypothesis that a lagged variable $X_{t-\tau}$ is independent of Y_t given the parents of Y_t selected with the causal

algorithm. However, we will see that our list of parents strongly coincides with the significant strong links identified in the second step.

4. Results & Discussion

We construct CEN for winter circulation and with different α and τ_{max} settings. Visualization of CEN as a process graph gives an easy to interpret picture of the underlying complex teleconnection pattern. Only the significant links are presented in the graph and the numbers next to the links stand for the associated time lag τ. Instantaneous links are represented by dashed links and have no direction or time-shift. The node color (in case the variable influences itself) and the link color represent the standardized regression coefficient (beta values) and hence capture the strength of the causal relationship. If two processes are linked for more than one time-lag then all lags are given (sorted by strength) with the link color based on the strongest connection. The time-lag for auto-driven data is not shown in the graph, but predominantly actors are lag-1 auto-correlated.

For the settings α=0.01, τ_{max}= 3 and using monthly data we obtain the CEN as in figure 5a. We find evidence that Barents Kara sea ice concentrations (BK-SIC) have a negative effect on sea level pressure over the Ural Mountains region (Ural-SLP) with a time-delay of three months. Thus, low sea ice in autumn can lead to increased surface pressure in winter. We also find a positive link from Ural-SLP to v-flux with a delay of one month which means that higher surface

pressure can increase the poleward heat flux, respectively the vertical wave activity. This is consistent with the mechanisms proposed by Cohen et al. (2014) and Kim et al. (2014). Moreover we can see in figure 5a, that increasing vertical wave activity induces a weakening of the stratospheric polar vortex with a delay of one month. Hence, the CEN depicts the Troposphere-Stratosphere coupling described by Kim et al. (2014) and Cohen et al. (2014). We also see a reverse relation from the Stratosphere into the Troposphere, whereby a weak polar vortex (PoV) leads to increasing sea ice in the Barents and Kara Seas and to less vertical wave activity. We find no causal link connecting a weak polar vortex to a negative AO. However, we have a positive instantaneous link between them, which might indicate that this connection is happening on a sub-monthly time-scale. In addition to the mechanisms involving the Stratosphere we also detect a direct positive link from BK-SIC to AO. Thus, we find that Barents and Kara sea ice in fall induces a weakening of AO in winter without any stratospheric connection. However, AO is also instantaneously related to sea level pressure in the Ural Mountains region (Ural-SLP) with a negative sign which is in turn strongly positively related with sea level pressure in Siberia (Sib-SLP). Even though the instantaneous links provide no direction, they are in accordance with the expectation that AO is negative when sea level pressure in the Arctic is high. The same is true for the instantaneous link connecting Sib-SLP and Ural-SLP to each other resp. to BK-SIC. In addition to the influence of Ural-SLP on PoV via v-flux we also find a weaker direct causal link between them with a delay of one month, suggesting that high sea level pressure in Central Asia can induce a weakening of the polar vortex directly, or via processes which are not part of the tested hypothesis. The positive instantaneous link between EA-snow and Sib-SLP is indicating that increasing snow cover in Eurasia is associated to a

strengthened Siberian High which is consistent with the hypothesis of Cohen et al. (2014). The auto-regressive influence (with a time-lag of one month) is as expected especially high for BK-SIC and EA-snow and weaker for PoV and AO. Ural-SLP, Sib-SLP and v-flux are not significantly causally influenced by their values in the months before.

We performed sensitivity analyses of the CEN to the parameter settings used and found the detected links to be robust. We limit ourselves to analyzing only links which go back to late summer. Figure 5 shows the winter months CENs associated with different significance levels (α = 0.01, 0.025, 0.05 in the rows) and for maximum time-lags of three and five months (columns). Not surprisingly, the number of significant links increases when we increase α, most of them involving the two actors based on sea level pressure (Fig. 5b, e, c, f). Also links associated with time-lags of more than three months (Fig. 5d-f) appear when increasing the maximum time-lag τ_{max}, however only for larger α values. We see that all links in Fig. 5a appear in all other graphs as well. For a significance level α>0.01 (Fig. 5b, e, c, f), we see that decreasing sea ice concentrations in the Barents and Kara Seas (BK-SIC) induce stronger sea level pressure over Siberia (Sib-SLP) with a lag of two months. This is in accordance with the mechanism described by Kim et al. (2014). We also see for α>0.01 that increasing snow cover in Eurasia (EA-snow) is also instantaneously positively linked to surface pressure over the Ural Mountains region (Ural-SLP). For a longer time lag we find that EA-snow is negatively influencing sea level pressure in the Ural Mountains region (Ural-SLP) with a delay of five months (Fig. 5e, f). For α=0.05 we even find some evidence that EA-snow can influence AO directly, and thus it seems again that processes not involving the Stratosphere are present. Overall, the CEN structure as in figure 5a appears for all tested parameters.

As explained in the method section, instantaneous links provide no information on the direction. To gain further information on the direction of those links and to further test the robustness of our findings, we construct CENs also for half-monthly and quarter-monthly time-series (see Fig. 6a, b). Since the data sets are then two-times respectively four-times longer and consist of shorter time-steps we adjust our settings for the CEN-algorithm. In order to make the results comparable with figure 5a we therefore double respectively quadruple τ_{max} to refer to the same time-shift. Since for higher time-resolutions more potential links are tested for significance we adjust the α value accordingly[6]. Comparing figure 5a with CENs based on half-monthly (Fig. 6a) and quarter-monthly (Fig. 6b) time series with the same maximum time-shift of three months and an adjusted significance level α=0.005625 for half-monthly and α=0.003 for quarter-monthly data, we find a robust pattern of the involved causal processes. Especially the Troposphere-Stratosphere connection is clearly visible in all CENs. For the CEN based on half-monthly data (Fig. 6a) the connection to vertical wave propagation (v-flux) is via the Siberian region (Sib-SLP) whereby this region is directly influenced by the Ural Mountains (Ural-SLP) area. On a quarter-monthly time-scale both regions directly influence v-flux which in turn influences PoV (Fig. 6b). On the other hand we have a direct link from PoV to AO (Fig. 6b) in the quarter-monthly based CEN, which indicates that a breakdown of the polar vortex causes a negative AO on a weekly time-scale. Also, there are direct links connecting Ural-SLP to EA-snow, BK-SIC and Sib-SLP, which shows that the Ural Mountains region has a strong influence on the surrounding

[6] If n denotes the number of actors, then $N= n^2(\tau_{max} + 1) - n$ potential links are tested. Thus, N=189 (monthly), N=336 (half-monthly) and N=630 (quarter-monthly). To calculate the adapted α we use a simple Bonferroni-correction and divide α=0.01 by the multiplicity of the performed tests.

regions on sub-monthly time-scales, which is in accordance with the tested hypothesis. However, the strong instantaneous links between tropospheric based actors (AO, Ural-SLP, Sib-SLP and EA-snow) remain for all time-scales, indicating that those causal processes are occurring on sub-weekly time-scales or are due to common drivers. The darker node-colors show that at sub-monthly time scales auto-regressive processes become larger.

In summary, the CEN-algorithm provides robust results, whereby additional links can predominantly be explained by changing parameter settings and by the temporal resolution of the underlying time-series. Barents and Kara sea ice (BK-SIC) is detected to play an important role on winter-circulation, especially on the monthly time-scale (Fig. 5) being responsible for changes in the pressure profile over the Ural Mountains region as well as by influencing AO directly. Thus, mechanisms effecting AO not involving the Stratosphere seem to be important, too. We assume that other processes for example as described by Petoukhov and Semenov [*Petoukhov and Semenov*, 2010] not represented by our choice of actors play a role, connecting Arctic sea ice and AO. As stated by Cohen and Kim, we find a connection of surface pressure (Ural-SLP) and upward wave activity (v-flux) into the Stratosphere for all parameter settings and time-scales (Fig. 5, 6). On lower time-scales we also have a direct link from Sib-SLP to v-flux (Fig. 6). These findings confirm the hypothesis that higher pressure over Central Asia leads to increasing vertical wave activity into the Stratosphere [*Cohen et al.*, 2014]. The Ural Mountains region as a preferred location for atmospheric blocking [*Wang et al.*, 2009] seems to play a central role for winter circulation, being linked to the tropospheric actors AO, BK-SIC, Sib-SLP and EA-snow on all time-scales. Further, the region is responsible for coupling with the Stratosphere (Fig. 5, 6). In this context, we expect that the link connecting Ural-SLP to PoV

directly, and not via v-flux, can at least partly be explained by hemispheric-wide averaging of the actors v-flux and PoV (in contrast to the regional actor Ural-SLP). Additionally, it is possible that a common driver not included in this analysis is responsible for this direct link. For example, tropical teleconnections like ENSO could influence both the Arctic Stratosphere and sea level pressure in Central Asia [*Butler et al.*, 2014]. Additionally, we find that the increased vertical wave activity can induce a weakening of the polar vortex (PoV), whereas PoV is positively connected to surface AO (Fig. 5, 6). Thus, our findings are consistent with the Troposphere-Stratosphere-Troposphere mechanisms described by Cohen et al. (2014) and Kim et al. (2014). We also find a reverse connection, linking a weak polar vortex (PoV) to increasing Barents and Kara sea ice and decreasing vertical wave activity (v-flux). This provides a negative feedback on a time-scale of approximately one to two months. The role of Eurasia snow cover (EA-snow) seems to be more complex. We find no evidence that late autumn snow fall in Eurasia influences the sea level pressure in Central Asia as proposed by Cohen et al. (2014). However, we find that EA-snow is instantaneously linked to Sib-SLP with positive sign and for $\alpha>0.01$ also to Ural-SLP (Fig. 5, 6). On a monthly time-scale we also have a direct negative link to Ural-SLP (with a lag of five months) and for $\alpha=0.05$ also to AO (with a lag of two months). Overall our findings are less robust for EA-snow.

5. Conclusion

In the context of hypothesis testing, we constructed *Causal Effect Networks* (CEN) in order to unravel causal relationships and their time delays between different actors of mid-latitude winter circulation. We restricted ourselves to studying Arctic mechanisms, based on those proposed by Kim et al. (2014) and Cohen et al. (2014). For each of the seven actors we constructed one index at different temporal resolutions. CEN-construction was performed by first deriving a set of parents for each actor, consisting of the conditional dependent processes (Step 1). Then those parents were used to estimate the strength and statistical significance of links employing linear regression models (Step 2). We only considered effects on winter circulation and applied the method to monthly, half-monthly and quarter-monthly time-series. We found that the method provides robust results for different values of the significance level α and maximum time delay τ_{max} as well as for the considered range of temporal resolutions.

Figure 7 (respectively Fig. 5a) contains the most robust links on a monthly scale whereby results are presented according to the approximate geographical location of the actors. Overall, our findings are largely consistent with previously proposed hypotheses under consideration, whereby especially Barents and Kara sea ice is detected to be an important external driver for winter circulation. Our CENs confirm the proposed Troposphere-Stratosphere coupling, which is evident for all tested parameter settings. However, we also find a robust pattern indicating a direct tropospheric connection of Barents and Kara sea ice and AO, such as for example proposed by Petoukhov and Semenov (2010). The direct link connecting Ural-SLP to PoV might be due to not considered tropical mechanisms influencing both the Stratosphere and sea level pressure in Eurasia as documented by Butler et al. (2014). The role of Eurasia snow cover is less robust but seems to influence sea level pressure in Asia significantly.

Since the CEN-algorithm requires the choice of the free parameters τ_{max} and α and depends on the temporal resolution of the underlying data, changing settings can produce different graphs. However, by including sensitivity tests for different parameter settings and time scales, we report robust results. Also, it should be noted that the CEN approach assumes stationary time-series. Long term trends or changing trends within the studied time period might affect the results [*Overland and Wang*, 2005] and require a careful treatment of the data. However, here we only found a clear negative linear trend in the sea ice data. The causal interpretation of the resulting CENs also depends on the choice of actors such that the inferred parents can still be due to not-yet-included other variables. The challenge of how to choose adequate actors can also be assessed by different methods such as dimension reduction via Principal Component Analysis [*Runge et al.*, 2015]. Nonetheless, the CEN-algorithm is especially useful for testing hypothesis if consistency of the data choice is assured.

The scope of this paper was to introduce and explain the CEN-algorithm and how it can be applied to address questions associated with teleconnections in the global climate system. In this context, CENs can overcome ambiguities of correlation analyses and provide a practical supplemental method to model experiments in order to test hypothesis. Moreover, CENs could be used also on model data to assess their validity. Here we limited ourselves to linear measurements, but CENs can also be constructed using non-parametric approaches, e.g., from information theory [*Runge et al.*, 2012a, 2012b]. Further research should address the question of how tropical mechanisms contribute to mid-latitude winter circulation [*Palmer*, 2014; *Trenberth et al.*, 2014] and also the different hypotheses related to summer circulation [*Overland et al.*, 2012; *Coumou et al.*, 2015].

Acknowledgements

The authors thank the editor and three anonymous reviewers for constructive and insightful comments that helped to significantly improve the manuscript. The work was supported by the German Federal Ministry of Education and Research (grant no. 01LN1304A). J.R. received support by the German Federal Ministry of Science and Education (Young Investigators Group CoSy-CC², grant no. 01LN1306A). J.F.D. thanks the Stordalen Foundation (via the Planetary Boundary Research Network PB.net) and the Earth League's EarthDoc program for financial support.

REFERENCES

Barnes, E. A., and J. A. Screen (2015), The impact of Arctic warming on the midlatitude jet-stream: Can it? Has it? Will it?, *Wiley Interdiscip. Rev. Clim. Chang.*, *6*, 277–286, doi:10.1002/wcc.337.

Butler, A. H., L. M. Polvani, and C. Deser (2014), Separating the stratospheric and tropospheric pathways of El Niño–Southern Oscillation teleconnections, *Environ. Res. Lett.*, *9*(2), 024014, doi:10.1088/1748-9326/9/2/024014.

Cohen, J., M. Barlow, P. J. Kushner, and K. Saito (2007), Stratosphere–Troposphere Coupling and Links with Eurasian Land Surface Variability, *J. Clim.*, *20*(21), 5335–5343, doi:10.1175/2007JCLI1725.1.

539 Cohen, J., J. Jones, J. C. Furtado, and E. Tziperman (2013), Warm Arctic, Cold Continents,
540 *Oceanography*, *26*(4), 1–12, doi:10.5670/oceanog.2013.70.

541 Cohen, J., J. C. Furtado, J. Jones, M. Barlow, D. Whittleston, and D. Entekhabi (2014a), Linking
542 Siberian snow cover to precursors of stratospheric variability, *J. Clim.*, *27*(14), 5422–5432,
543 doi:10.1175/JCLI-D-13-00779.1.

544 Cohen, J. et al. (2014b), Recent Arctic amplification and extreme mid-latitude weather, *Nat.*
545 *Geosci.*, *7*, 627–637, doi:10.1038/ngeo2234.

546 Coumou, D., V. Petoukhov, S. Rahmstorf, S. Petri, and H. J. Schellnhuber (2014), Quasi-resonant
547 circulation regimes and hemispheric synchronization of extreme weather in boreal
548 summer, *Proc. Natl. Acad. Sci.*, *111*(34), 12331–12336, doi:10.1073/pnas.1412797111.

549 Coumou, D., J. Lehmann, and J. Beckmann (2015), The weakening summer circulation in the
550 Northern Hemisphere mid-latitudes, *Science (80-.).*, doi:10.1126/science.1261768.

551 Deng, Y., and I. Ebert-Uphoff (2014), Weakening of atmospheric information flow in a warming
552 climate in the Community Climate System Model, *Geophys. Res. Lett.*, *41*(1), 193–200,
553 doi:10.1002/2013GL058646.

554 Deser, C., R. Tomas, M. Alexander, and D. Lawrence (2010), The Seasonal Atmospheric Response
555 to Projected Arctic Sea Ice Loss in the Late Twenty-First Century, *J. Clim.*, *23*, 333–351,
556 doi:10.1175/2009JCLI3053.1.

557 Ebert-Uphoff, I., and Y. Deng (2012), Causal discovery for climate research using graphical
558 models, *J. Clim.*, *25*(17), 5648–5665, doi:10.1175/JCLI-D-11-00387.1.

559 Francis, J. A., and S. J. Vavrus (2012), Evidence linking Arctic amplification to extreme weather in
560 mid-latitudes, *Geophys. Res. Lett.*, *39*(6), doi:10.1029/2012GL051000.

561 Furtado, J. C., J. L. Cohen, A. H. Butler, E. E. Riddle, and A. Kumar (2015), Eurasian snow cover
562 variability and links to winter climate in the CMIP5 models, *Clim. Dyn.*, *45(9)*,
563 doi:10.1007/s00382-015-2494-4.

564 Gray, S. L., C. M. Dunning, J. Methven, G. Masato, and J. M. Chagnon (2014), Systematic model
565 forecast error in Rossby wave structure, *Geophys. Res. Lett.*, *41*(8), 2979–2987,
566 doi:10.1002/2014GL059282.

567 Handorf, D., R. Jaiser, K. Dethloff, A. Rinke, and J. Cohen (2015), Impacts of Arctic sea-ice and
568 continental snow-cover changes on atmospheric winter teleconnections, *Geophys. Res.*
569 *Lett.*, *42*(7), doi:10.1002/2015GL063203.

570 Jaiser, R., K. Dethloff, D. Handorf, A. Rinke, and J. Cohen (2012), Impact of sea ice cover changes
571 on the Northern Hemisphere atmospheric winter circulation, *Tellus A*, *64*,
572 doi:10.3402/tellusa.v64i0.11595.

573 Kim, B.-M., S.-W. Son, S.-K. Min, J.-H. Jeong, S.-J. Kim, X. Zhang, T. Shim, and J.-H. Yoon (2014),
574 Weakening of the stratospheric polar vortex by Arctic sea-ice loss, *Nat. Commun.*, *5*,
575 doi:10.1038/ncomms5646.

576 Manzini, E. et al. (2014), Northern winter climate change: Assessment of uncertainty in CMIP5
577 projections related to stratosphere-troposphere coupling, *J. Geophys. Res. Atmos.*, *119*(13),
578 7979–7998, doi:10.1002/2013JD021403.

579 Overland, J. E., and M. Wang (2005), The Arctic climate paradox: The recent decrease of the
580 Arctic Oscillation, *Geophys. Res. Lett.*, *32*(6), L06701, doi:10.1029/2004GL021752.

581 Overland, J. E., J. A. Francis, E. Hanna, and M. Wang (2012), The recent shift in early summer
582 Arctic atmospheric circulation, *Geophys. Res. Lett.*, *39*(19), doi:10.1029/2012GL053268.

583 Palmer, T. (2014), Record-breaking winters and global climate change, *Science (80-.).*,
584 *344*(6186), 803–804, doi:10.1126/science.1255147.

585 Palmer, T. N., and D. A. Mansfeld (1984), Response of 2 atmospheric general circulation models
586 to sea-surface temperature anomalies in the tropical East and West Pacific, *Nature*, *310*,
587 485–485, doi:10.1038/310483a0.

588 Palmer, T. N., and J. A. Owen (1986), A possible relationship between some “severe” winters in
589 North America and enhanced convective activity over the tropical west Pacific, *Mon.*
590 *Weather Rev.*, *114*(3), 648–651, doi:10.1175/1520-
591 0493(1986)114<0648:APRBSW>2.0.CO;2.

592 Pearl, J. (2013), Linear Models: A Useful “Microscope” for Causal Analysis, *J. Causal Inference*,
593 *1*(1), 155–170, doi:10.1515/jci-2013-0003.

594 Petoukhov, V., and V. A. Semenov (2010), A link between reduced Barents-Kara sea ice and cold
595 winter extremes over northern continents, *J. Geophys. Res. Atmos.*, *115*(D21),
596 doi:10.1029/2009JD013568.

Polvani, L. M., and D. W. Waugh (2004), Upward Wave Activity Flux as a Precursor to Extreme Stratospheric Events and Subsequent Anomalous Surface Weather Regimes, *J. Clim.*, *17*(18), 3548–3554, doi:10.1175/1520-0442(2004)017<3548:UWAFAA>2.0.CO;2.

Robinson, D. A., K. F. Dewey, and R. R. Heim (1993), Global Snow Cover Monitoring: An Update, *Bull. Am. Meteorol. Soc.*, *74*(9), 1689–1696, doi:10.1175/1520-0477(1993)074<1689:GSCMAU>2.0.CO;2.

Runge, J., J. Heitzig, V. Petoukhov, and J. Kurths (2012a), Escaping the curse of dimensionality in estimating multivariate transfer entropy, *Phys. Rev. Lett.*, *108*(25), 258701, doi:10.1103/PhysRevLett.108.258701.

Runge, J., J. Heitzig, N. Marwan, and J. Kurths (2012b), Quantifying causal coupling strength: A lag-specific measure for multivariate time series related to transfer entropy, *Phys. Rev. E*, *86*(6), 61121, doi:10.1103/PhysRevE.86.061121.

Runge, J., V. Petoukhov, and J. Kurths (2014), Quantifying the strength and delay of climatic interactions: The ambiguities of cross correlation and a novel measure based on graphical models, *J. Clim.*, *27*(2), 720–739, doi:10.1175/JCLI-D-13-00159.1.

Runge, J., V. Petoukhov, J. F. Donges, J. Hlinka, N. Jajcay, M. Vejmelka, D. Hartman, N. Marwan, and M. Paluˇ (2015), Identifying causal gateways and mediators in complex spatio-temporal systems, *Nat. Commun.*, *8*, doi:10.1038/ncomms9502.

Schleussner, C. F., J. Runge, J. Lehmann, and A. Levermann (2014), The role of the North Atlantic overturning and deep ocean for multi-decadal global-mean-temperature variability, *Earth Syst. Dyn.*, *5*(1), 103–115, doi:10.5194/esd-5-103-2014.

Screen, J. A., and I. Simmonds (2014), Amplified mid-latitude planetary waves favour particular regional weather extremes, *Nat. Clim. Chang.*, doi:10.1038/NCLIMATE2271.

Spirtes, P., C. Glymour, and R. Scheines (2000), *Causation, Prediction, and Search*.

Thompson, D. W. J. (2001), Regional Climate Impacts of the Northern Hemisphere Annular Mode, *Science (80-.).*, *293*(5527), 85–89, doi:10.1126/science.1058958.

Tremblay, L. B., M. M. Holland, I. V. Gorodetskaya, and G. A. Schmidt (2007), An Ice-Free Arctic? Opportunities for Computational Science, *Comput. Sci. Eng.*, *9*(3), 65–74, doi:10.1109/MCSE.2007.45.

Trenberth, K. E., G. W. Branstator, D. Karoly, A. Kumar, N.-C. Lau, and C. Ropelewski (1998), Progress during TOGA in understanding and modeling global teleconnections associated with tropical sea surface temperatures, *J. Geophys. Res.*, *103*(C7), 14291, doi:10.1029/97JC01444.

Trenberth, K. E., J. T. Fasullo, G. Branstator, and A. S. Phillips (2014), Seasonal aspects of the recent pause in surface warming, *Nat. Clim. Chang.*, *4*(10), 911–916, doi:10.1038/nclimate2341.

Wang, L., W. Chen, W. Zhou, J. C. L. Chan, D. Barriopedro, and R. Huang (2009), Effect of the climate shift around mid 1970s on the relationship between wintertime Ural blocking circulation and East Asian climate, *Int. J. Climatol.*, *30*, 153–158, doi:10.1002/joc.1876.

Tables

Abbreviation	Actor	Variable/Unit	Region (Level)
BK-SIC	Barents Kara sea ice	Sea ice area fraction	70 °- 80°N, 30°- 105°E
EA-snow	Eurasia snow cover	snow covered area fraction	40° - 80°N, 30°-180°E
AO	Arctic Oscillation Index	Geopotential height in m	20° - 90°N (1000 mb)
v-flux	Vertical wave propagation	Pole-ward eddy heat flux v*T* in K*m/s	45° - 75°N (100 mb)
PoV	Polar Vortex	Geopotential height in m	65° - 90°N (10 - 100 mb)
Sib-SLP	Siberian High	Sea level pressure in mb	40° - 65°N, 85° - 120°E
Ural-SLP	Ural Mountains sea level pressure	Sea level pressure in mb	45° - 70°N, 40° - 85°E

Table 1: Table of variables and regions of every considered actor

Actor	Parents $\mathcal{P}$
AO	AO_{t-1}, BK-SIC_{t-2}
BK-SIC	BK-SIC_{t-1}, PoV_{t-2}
EA-snow	EA-$snow_{t-1}$
v-flux	PoV_{t-1}
PoV	v-$flux_{t-1,}$ Ural-SLP_{t-1}, PoV_{t-1}
Sib-SLP	None
Ural-SLP	BK-SIC_{t-3}

Table 2: Table of parent processes of each actor for winter (DJF) data and with the settings α=0.01 and τ_{max}=3. The subscript denotes the time lag in months. The parent processes are then used in the second step of the CEN-algorithm in order to quantify the link strength in terms of linear regression coefficients.

FIGURE CAPTIONS

Figure 1: Schematic picture of different time scales, whereby each box indicates one time-step. Quarter-monthly time series (bottom row) consists of four times respectively two times more data points than monthly (top row) and half-monthly (middle row) time series.

Figure 2: Monthly time-series of all calendar months of climatological anomalies of each actor from 01/1979-12/2014.

Figure 3: Possible scenarios leading to a correlation without a direct causation between process X and Y: a) inflated correlation due to autocorrelation b) indirect chain via Z c) common driver Z.

Figure 4: Schematic picture of time series considered to measure influence of actor X on winter polar vortex (PoV) with a time-lag $\tau=1$, whereby the time-series only consist of the dark grey boxes.

Figure 5: CENs of actors of winter (DJF) circulation based upon monthly mean data. With a maximum time-lag of $\tau_{max}= 3$ (a, b, c) and $\tau_{max}= 5$ (d, e, f) and with significance level $\alpha=0.01$ (a, d), $\alpha=0.025$ (b, e) and $\alpha=0.05$ (c, f).

Figure 6: CEN of actors of winter (DJF) circulation for a) half-monthly data with $\tau_{max} =6$ and $\alpha=0.005625$ and b) quarter-monthly data with $\tau_{max} =12$ and $\alpha=0.003$.

Figure 7: Same as Fig. 5a but the network is embedded in a schematic projection of the earth and the atmosphere. The regional actors BK-SIC, Ural-SLP, Sib-SLP and EA-snow are presented according to their approximate geographical location and the hemispheric actors AO, v-flux and PoV are presented according to their approximate latitude and pressure levels. See Tab. 1 for the exact coordinates of all actors.

FIGURES

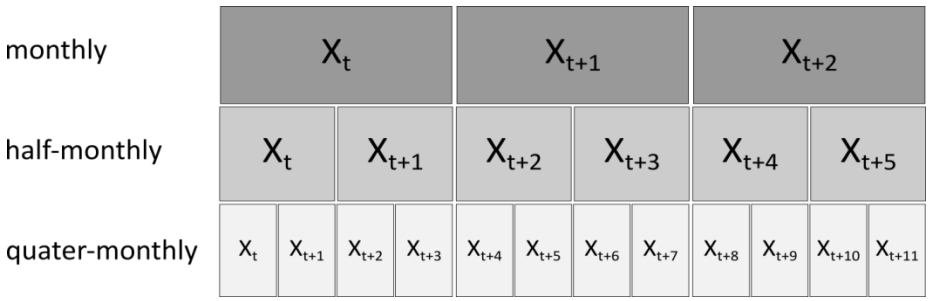

Figure 1: *Schematic picture of different time scales, whereby each box indicates one time-step. Quarter-monthly time series (bottom row) consists of four times respectively two times more data points than monthly (top row) and half-monthly (middle row) time series.*

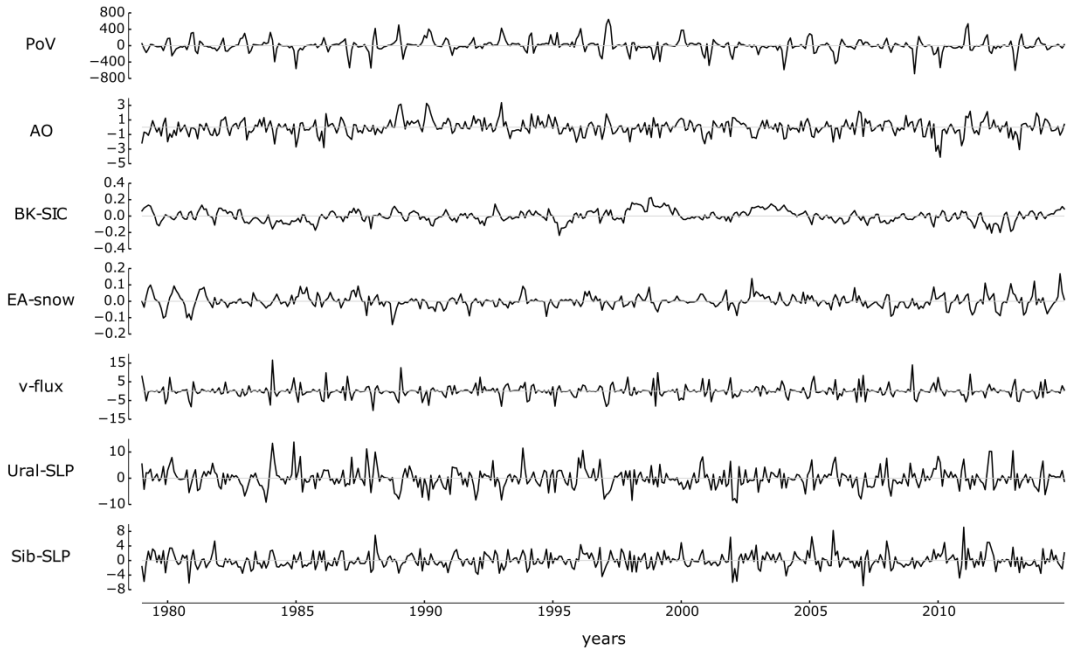

Figure 2: *Monthly time-series of all calendar months of climatological anomalies of each actor from 01/1979-12/2014.*

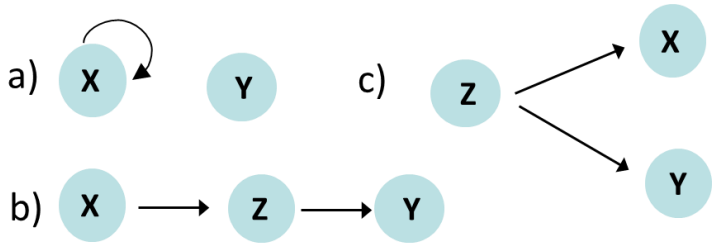

Figure 3: *Possible scenarios leading to a correlation without a direct causation between process X and Y: a) inflated correlation due to autocorrelation b) indirect chain via Z c) common driver Z.*

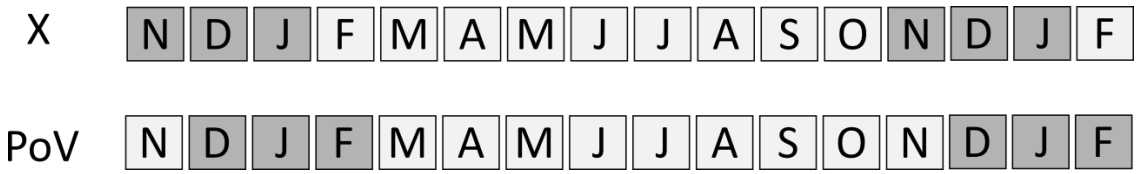

Figure 4: *Schematic picture of time series considered to measure influence of actor X on winter polar vortex (PoV) with a time-lag τ=1, whereby the time-series only consist of the dark grey boxes.*

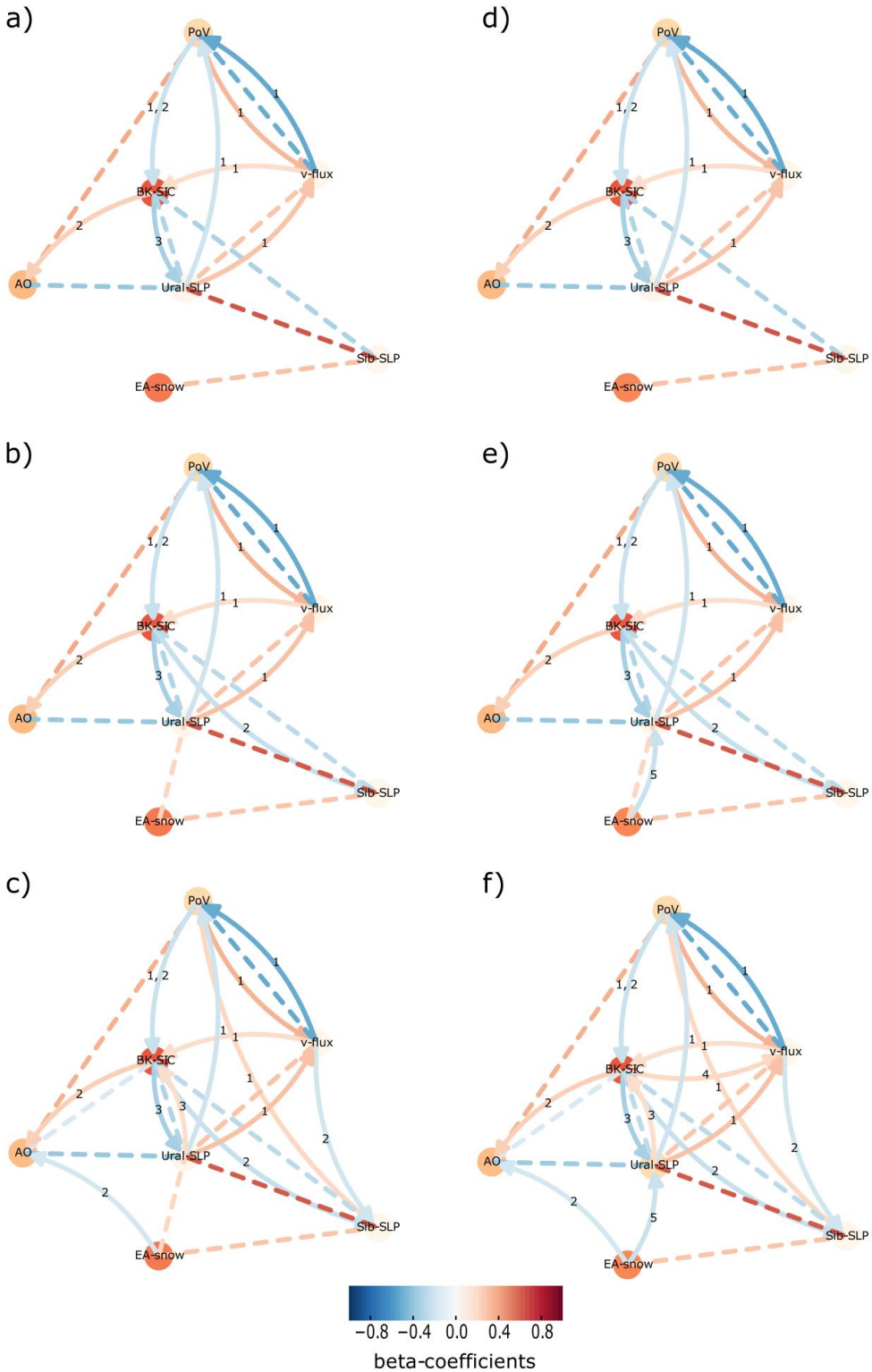

Figure 5: *CENs of actors of winter (DJF) circulation based upon monthly mean data. With a maximum time-lag of* τ_{max}*= 3 (a, b, c) and* τ_{max}*= 5 (d, e, f) and with significance level α=0.01 (a, d), α=0.025 (b, e) and α=0.05 (c, f).*

707

708

709

710

711

712

713

714

715

716

717

718

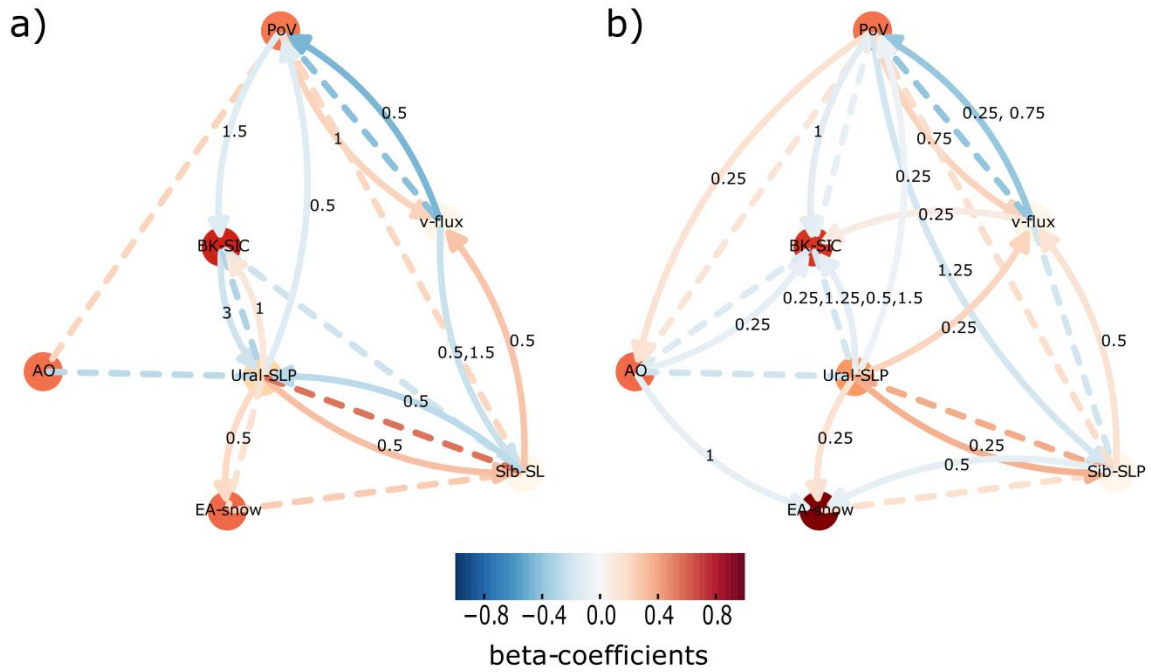

719

720

721 ***Figure 6:*** *CEN of actors of winter (DJF) circulation for a) half-monthly data with* τ_{max} *=6 and* α*=0.005625 and b)*

722 *quarter-monthly data with* τ_{max} *=12 and* α*=0.003.*

723

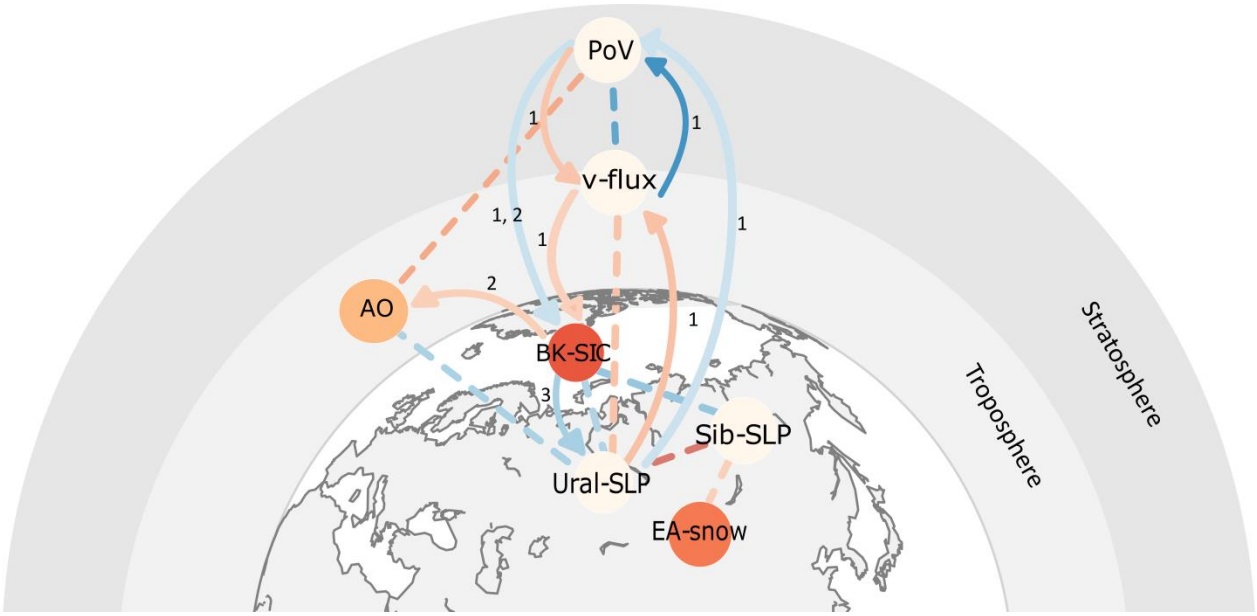

Figure 7: *Same as Fig. 5a but the network is embedded in a schematic projection of the earth and the atmosphere. The regional actors BK-SIC, Ural-SLP, Sib-SLP and EA-snow are presented according to their approximate geographical location and the hemispheric actors AO, v-flux and PoV are presented according to their approximate latitude and pressure levels. See Tab. 1 for the exact coordinates of all actors.*